

RSC Advances

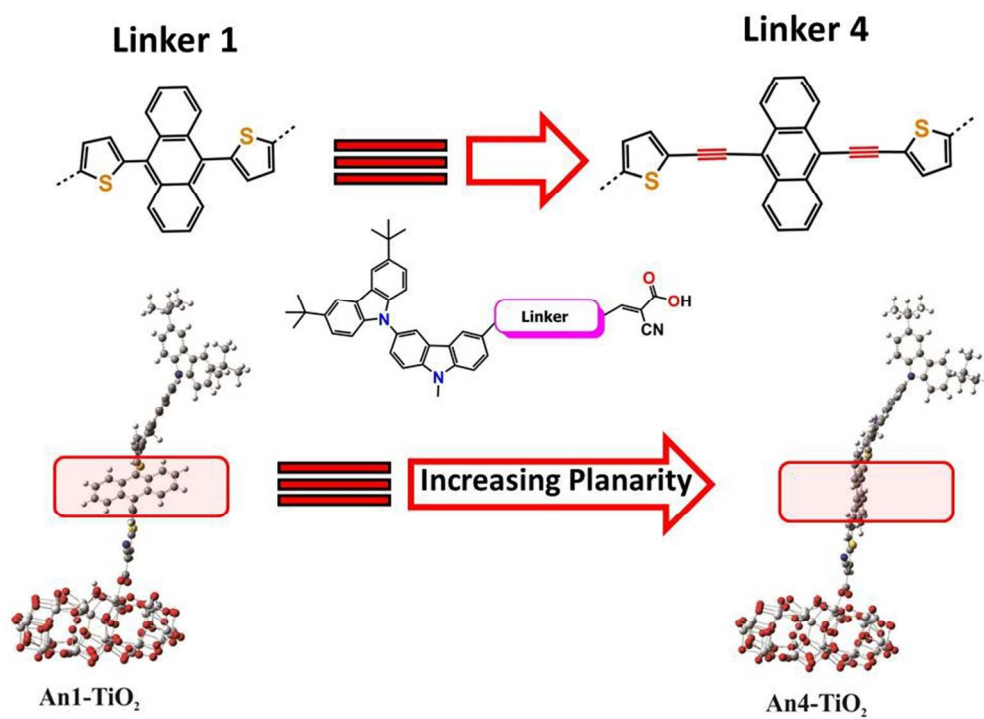


This is an *Accepted Manuscript*, which has been through the Royal Society of Chemistry peer review process and has been accepted for publication.

Accepted Manuscripts are published online shortly after acceptance, before technical editing, formatting and proof reading. Using this free service, authors can make their results available to the community, in citable form, before we publish the edited article. This *Accepted Manuscript* will be replaced by the edited, formatted and paginated article as soon as this is available.

You can find more information about *Accepted Manuscripts* in the [Information for Authors](#).

Please note that technical editing may introduce minor changes to the text and/or graphics, which may alter content. The journal's standard [Terms & Conditions](#) and the [Ethical guidelines](#) still apply. In no event shall the Royal Society of Chemistry be held responsible for any errors or omissions in this *Accepted Manuscript* or any consequences arising from the use of any information it contains.



254x190mm (96 x 96 DPI)

Triple Bond-Modified Anthracene Sensitizers for Dye-Sensitized Solar Cells: A Computational Study

Ruangchai Tarsang¹, Vinich Promarak², Taweesak Sudyoasuk¹, Supawadee Namuangruk³,
Nawee Kungwan⁴, Siriporn Jungsuttiwong^{1,*}

¹Center for Organic Electronic and Alternative Energy, Department of Chemistry and Center of Excellence for Innovation in Chemistry, Faculty of Science, Ubon Ratchathani University, Ubon Ratchathani 34190, Thailand

²School of Chemistry and Center of Excellence for Innovation in the Chemistry, Institute of Science, Suranaree University of Technology, Nakhon Ratchasima 30000, Thailand

³National Nanotechnology Center, National Science and Technology Development Agency, Klong Luang, Pathumthani 12120, Thailand

⁴Department of Chemistry, Faculty of Science, Chiang Mai University, Chiang Mai 50200, Thailand

* All correspondence should be addressed to S. Jungsuttiwong: Email: siriporn.ubu@gmail.com.

Tel.: +664 535 3400 ext.4510, Fax: +664 528 8379

ABSTRACT

We performed a theoretical investigation on a series of organic dyes incorporating an anthracene moiety between a carbazole donor group and a cyanoacrylic acid acceptor, in which a triple bond (TB)-modified moiety acts as a π -conjugated linker. Density functional theory (DFT) and time-dependent DFT (TD-DFT) were applied to understand the electronic, photophysical, and electron injection properties of the dyes. We found that optimized anthracene structures lay almost perpendicular to the plane of the adjacent substituents. The introduction of a modified TB moiety significantly decreases the dihedral angle and results in a planar structure, which extends the length of π -conjugated system to provide a broader absorption spectrum, the **An4** dye exhibited the greatest red shift in maximum absorption wavelength. Introduction of a TB moiety into the dye structure facilitates electron transfer from the donor and acceptor. The TB-modified dye structure has a significant effect on electron injection from the dye sensitizer to the TiO₂ surface. Our results demonstrate that use of computational design can help the experimentalist for out looking future developments to identify TB-modified anthracene sensitizers for highly efficient solar cells.

Keywords: Anthracene, Triple bond, Linker Bridge, Dye-sensitized solar cells, Density functional theory

1. Introduction

DSSCs have received extensive attention since the first report of high-efficiency dye-sensitized solar cells (DSSC) by O'Regan and Grätzel in 1991,¹ DSSC manufacture requires relatively low-cost, facile processes compared to traditional silicon-based solar cells. Thus, the conversion of sunlight to electricity using DSSCs is a promising source of affordable renewable energy.² During recent decades, there have been numerous reports of DSSC-based investigations, with over 1000 articles published by the end of the 20th century, and this trend continues to grow.³ Metal-free organic-dye-based sensitizers show promise for DSSC applications, and there is active experimental and theoretical research into the development of organic-dye-based DSSC cells with high solar-to-electricity conversion efficiency.⁴⁻⁶

The majority of research into metal-free organic dyes is concerned with the design of novel dye sensitizers, which are a key component in the DSSC working principle to harvest solar irradiation for converting light to electricity. The metal-free dye based on a donor- π -conjugated-acceptor (D- π -A) architecture can provide high-efficient photovoltaic performance,⁷ the highest record exceeding 11%.⁸ A variety of electron donating groups (D) have been reported, including triarylamine,⁹ coumarin,¹⁰ carbazole,¹¹ fluorine,¹² and phenothiazine.^{13, 14} Three main electron acceptor groups (A) are used, namely, cyanoacrylic acid,¹⁵ carboxylic acid,¹⁶ and rhodanine-3-acetic acid.¹⁷

The presence of a π -conjugated linker in an organic sensitizer broadens the visible region absorption band by extending the length of the π -conjugation system. Structural modification of the π -conjugated linker can greatly improve DSSC performance.^{5, 18} Researchers have varied π -conjugated bridges by using a series of acenes comprising polycyclic aromatic hydrocarbons with fused benzene rings in a rectilinear arrangement. In particular, an anthracene moiety, which consists of three fused benzene rings, shows promise as an acene-modified linker. In recent years, Fan et al.¹⁹ reported a series of dye sensitizers

with acene-modified linkers, from benzene to pentacene. Fan reported that the presence of an anthracene unit provided several advantages, including good light-harvesting efficiency (*LHE*) and improved electron injection properties. Thus, anthracene shows promising as a linker component to provide a highly efficient dye sensitizer for DSSC applications. Additionally, the anthracene group outperforms other acene-modified linkers in the benzene to pentacene series,²⁰ with an overall efficiency of approximately 5.44%.

Generally, there are two ways to derivatize anthracene as a π -conjugated linker; substituent groups can be introduced at either the 9,10- or the 2,6-positions on the anthracene unit to provide alternative conjugation pathways. However, substitution at the 2,6-positions on anthracene is less thermodynamically favorable compared to 9,10-disubstitution, and there are few reports on the incorporation of substituents at the 2,6-positions.²¹⁻²³ Nonetheless, substitution at the 2,6-positions offers lower steric congestion than that seen for 9,10-disubstitution, and generally maintains better planarity with the rest of the conjugated system. A planar structure can provide a broader absorption spectrum, leading to better light harvesting performance.²⁴⁻²⁶ The majority of previous reports have focused on development of organic sensitizers containing 9,10-disubstituted anthracene moieties for DSSCs. For example, Thomas et al.²⁷ reported the preparation of dye sensitizers featuring 9,10-substituted anthracene linkers inserted between triarylamine-based donor and cyanoacrylic acid acceptor units via a conjugation pathway composed of thiophene and benzothiadiazole units. Teng et al.⁵ designed and synthesized a series of metal-free organic dyes bridged by a π -conjugation system containing anthracene. One of the reported dyes showed excellent power conversion efficiency of up to 7.03% under simulated AM 1.5 irradiation (100 mW/cm²). Heo et al.²⁵ reported the synthesis of various anthracene mediated π -conjugated dyes incorporating triple-bond and thiophene moieties for fine-tuning molecular configuration and for broadening the absorption spectrum. Liet al.²⁸ reported a series of

organic sensitizers featuring a 9,10-diaryl-substituted anthracene unit that facilitated the construction of high conversion efficiency solar cells. However, all of the reported 9,10-anthracene-based sensitizers suffered severe steric congestion between the anthracene core and the substituent aromatic rings. Therefore, relieving the steric congestion introduced by substitution at the 9,10-positions on anthracene has the potential to improve the power conversion efficiency of these organic-dye-based DSSCs.

Recently, Yan et al.²⁹ had studied on the introduction of triple bond (TB) moiety between an electron donor and π -conjugate linker. However, the triple-bond insertion on this way brings to reduce open-circuit photovoltage (V_{oc}) owing to faster interfacial charge recombination. On the other hand, Yang et al.³⁰ had employed TB inserted between π -conjugate linker and an electron acceptor. The results showed that better electron injection from the excited state resulting in significantly improved a short circuit photo current (J_{sc}). Thus, we believed that the triple-bond modification is an important consideration in the future dyes design.

Theoretical studies investigating the relationships between structure, and the properties and performance of dye sensitizers offer shorter development times and significant cost savings over traditional synthetic approaches. Accurate first-principle density functional calculations using supercomputing facilities are now commonly available to research groups.³¹⁻³³ Calculations are employed as a tool to design, study, and screen dye sensitizer candidates prior to synthesis. Computer-aided rational design of new dye sensitizers has recently seen reports from several groups,³⁴⁻³⁶ including our own group.³⁷⁻⁴¹

In this study, we aimed to develop anthracene-based dyes that incorporate a triple bond (TB)-modified π -conjugated linker to alleviate steric congestion between the anthracene moiety and its neighboring aromatic rings. We introduced thiophene units at the 9- and 10-

positions of an anthracene ring without TB-modification for dye **An1**, as a reference dye. For the **An2** dye, we introduced a TB connector between the 9-position on anthracene and the thiophene substituent. The **An3** dye incorporated a TB group at the 10-anthracene position, and the **An4** dye featured TB 9,10-disubstitution. The molecular structures of the **An1–An4** dyes are shown in **Figure 1**. Structural, optical, and electronic properties were investigated to identify the effects of the different TB-substitutions on the light harvesting properties of the dyes.

2. Computational details

All calculations on the structure and electronic properties of the isolated dyes have been performed with the GAUSSIAN 09 program.⁴² The ground state geometries of the modified **An1–An4** anthracene-based dyes were fully optimized using Density Functional Theory (DFT) with Becke's three-parameter hybrid function and Lee-Yang-Parr's gradient-corrected correlation function (B3LYP)⁴³ at the 6–31G(d,p) level.⁴⁴ All calculations were performed without symmetry constraints in the gas phase. Optimized structures were then be used to calculate excitation energy (E_g), maximum absorption wavelength (λ_{\max}), and oscillator strength (f) for the 10 lowest energy states in dichloromethane solvent (CH_2Cl_2), by applying Time-Dependent Density Functional Theory (TD-DFT) with CAM-B3LYP⁴⁵ at the 6-31G(d,p) level of theory. The TD-DFT results were entered into the SWizard program⁴⁶ for simulation of the dye absorption spectra.

To gain insight into the electron injection properties, the TiO_2 film were modeled with a stoichiometric anatase (101) surface as the $(\text{TiO}_2)_{38}$ cluster, which is similar to that described by Nazeeruddin et al.⁴⁷ This model by DFT calculations using the DMol³ program⁴⁸ in Materials Studio, version 5.5 has been widely used to study dye@ TiO_2 adsorption and represents a reasonable choice between accuracy and computational convenience, and nicely reproduces the main electronic characteristics of TiO_2 nanoparticles.^{37, 39, 49 38, 40, 50-53} The HOMO, LUMO and

HOMO–LUMO energy gap of the this cluster are calculated to be 27.98, 23.52, and 24.46 eV, respectively, while the lowest excitation is obtained as 3.75 eV³⁸ which is reasonably higher than typical band gaps of TiO₂ nanoparticles of a few nm size of 3.2–3.3 eV.^{54, 55} The TiO₂ conduction band edge was calculated at ca. -4 eV vs. vacuum, in good agreement with experimental values.⁵⁶ In addition, this cluster size has been comparatively tested with a relatively larger (TiO₂)₈₂ cluster and the both clusters shows a similar conduction band structure, within 0.1 eV, to the corresponding periodic model.⁵⁷ Therefore, this work we use the (TiO₂)₃₈ cluster for representing the TiO₂ surface for dye adsorption.

The (TiO₂)₃₈ configurations were fully optimized using the generalized gradient-corrected approximation (GGA) method. The Perdew–Burke–Ernzerhof (PBE) function was applied with the DNP basis set to account for exchange-correlation effects. The core electron was subjected to a DFT-SemicorePseudo Potential (DSPP). The criteria for the optimization threshold are similar those used in our previous reports.^{37-39, 41, 50} After optimization, adsorption energies (E_{ads}) of the dyes on (TiO₂)₃₈ clusters were obtained by **Equation 1**:

$$E_{ads} = E_{dye} + E_{TiO_2} - E_{dye+TiO_2} \quad (1)$$

Where E_{dye} is the total energy of the isolated dye, E_{TiO_2} is the total energy of the (TiO₂)₃₈ cluster, and $E_{dye+TiO_2}$ is the total energy of the dye-(TiO₂)₃₈ complex. Following calculation, a positive E_{ads} value indicates stable adsorption of the dye onto TiO₂.

3. Results and discussion

3.1 Optimized ground-state geometries

To gain insight into the molecular structures of the studied dyes, the ground-state geometries of dyes **An1–An4** were optimized using DFT at the B3LYP level with the 6-31G(d,p) basis set. The dyes are grouped into three parts as shown in **Figure 2a**: (i) two

carbazole groups (Cbz) acting as donor, (ii) different thiophene groups (Thi), an anthracene moiety (An), or a triple bond (TB) as linker, and (iii) cyanoacrylic acid (Cyn) as the acceptor. **Figure 2(b)** shows optimized ground-state geometries for **An1–An4**. **Table 1** summarizes the dye C-C bond lengths (r) and dihedral angles (ϕ). The calculated C-C bond lengths are identical for all dyes within the donor moiety (Cbz-Cbz) (1.42 Å), between the donor and linker (Cbz-Thi) (1.46 Å), and between the linker and acceptor (Thi-Cyn) (1.43 Å). The dihedral angles formed between the two donors (Cbz-Cbz) lie approximately 60° out-of-plane from each other, resulting in reduced dye-aggregation at the donor group. All of the calculated dihedral angles formed between the π -linker and the cyanoacrylic acid acceptor (Thi-Cyn) are close to zero and accordingly, these components are almost coplanar. To investigate the relationships between the various π -conjugated linkers and the charge transfer properties, we examined the critical dihedral angles on the linker moiety. From the side view of the studied dyes (**Figure 2b**), the presence of an anthracene moiety as linker-bridge in the **An1** dye, produces a large dihedral angle, with the anthracene and thiophene groups almost perpendicular at the 9,10-anthracene positions, providing significant steric effects and loss of planarity. Insertion of TB at position 9 on anthracene in **An2**, at position 10 in **An3**, and at both 9,10-positions in **An4**, significantly decreases the dihedral angles compared to the **An1** dye. These observations reveal that the presence of a triple bond decreases the dihedral angles at the 9,10-functionalized positions on anthracene, which in turn reduces steric hindrance, and increases planarity within the anthracene dye.

Furthermore, to describe the length of the conjugated bridge in the dye, we define “ L ” as the distance of coplanarity formed between π -conjugated linker and the cyanoacrylic acid acceptor. The side view in **Figure 2b** shows that distance L for the **An1** dye is approximately 8.18 Å. Substitution with TB at 9-position in the **An2** dye has little effect on L ; the distance is

similar to that seen for dye **An1**. Insertion of TB at position-10 in dye **An3** produces a significant increase in L , to 10.72 Å. This suggests that the presence of TB at the 10-functionalized position on anthracene extends the π -conjugation system. Position 10 is closer to the cyanoacrylic anchor than is the 9-position, which is positioned opposite to the acceptor group. Finally, the presence of TB groups at both the 9- and 10-positions in **An4** results in coplanarity between the anthracene moiety and the core molecule, and provides the longest L distance of 17.53 Å. The distance L is a key parameter for optimizing these anthracene based sensitizers.

3.2 Frontier molecular orbitals (FMOs)

To further explore the effects of different π -conjugated linkers on intramolecular charge transfer (ICT), we plotted the electron distributions in two frontier molecular orbitals: the highest occupied molecular orbitals (HOMO) and the lowest unoccupied molecular orbitals (LUMO). **Figure 3** illustrates the HOMO and LUMO frontier molecular orbitals, and the charge density differences ($\Delta\rho$) between ground and the excited states. An important characteristic of electron density in the frontier molecular orbitals is the overlap between the HOMO and LUMO. At LUMO of **An1** and **An2**, there are no electron distributions on anthracene unit indicating that the HOMO and LUMO do not overlap. This suggests that ICT would not occur across the anthracene unit for these dyes. From the **An3** and **An4** (**Figure 3**), the well-overlapped HOMO and LUMO orbitals extend across the anthracene π -linker, suggesting good induction and electron-withdrawing properties for the donor and acceptor, respectively. Thus, we anticipate that this strong-overlapping character will facilitate ICT between the donor and acceptor, subsequently toward to conduction band of TiO₂.

Furthermore, we perform the $\Delta\rho$ plots revealing electron density differences between the ground- and excited-states to provide further evidence for ICT. The decreased (purple)

mainly localized on the donor and linker parts, while the increased (yellow) electron densities localized on the anchoring group. In regards to the electron density delocalized throughout the entire molecular backbone, the ICT as well as the injection mechanism are possible when transition occurs for all dyes. The ICT property was generally accepted that is related to the dipole moment (μ) of the individual dye perpendicular to the surface of semiconductor. It is reasonable that the larger μ of the adsorbed dyes, the larger V_{oc} . Therefore, we performed dipole moment calculation under B3LYP/6-31G(d,p) level at the geometry of isolated dyes. The calculated total dipole moments (μ) are listed in **Table 2**. The total μ of dyes increases in the order of **An1** (6.30) < **An2** (7.25) < **An3** (7.47) < **An4** (9.52) as the planarity changes. The largest vertical dipole moment of **An4** dye is considered to provide the great ICT property.

3.3 Energy diagram

Figure 4 shows calculated HOMO and LUMO energy levels for dyes **An1–An4**. Importantly, the HOMO energy level is required to match with the redox potential of the iodine/triiodide (I/I_3^-) electrolyte system for suitable charge recombination back to the oxidized dyes, whereas the LUMO level is required to match with the TiO_2 conduction band (CB) edge for efficient injection of excited electrons. For LUMO levels, the criterion for an efficient electron injection process requires that the energy gap between the LUMO and the CB edge of TiO_2 is greater than approximately 0.2 eV.¹⁷ As shown in **Figure 4**, the simulated LUMO levels are -2.89, -3.14, -2.96, and -3.12 eV for **An1–An4** respectively, which are greater magnitude than the CB of $(TiO_2)_{38}$ cluster of -4.00 eV in the experiment. The energy gaps between the acceptor LUMO and TiO_2 CB calculated to be 0.61, 0.36, 0.54, and 0.38 eV for the **An1–An4** dyes, respectively, indicating that injection of excited electrons from the dye excited-state into the TiO_2 conduction band edge should be thermodynamically favorable.

For HOMO level, HOMO energy levels must lie below the I^-/I_3^- redox couple (-4.80 eV)^{58, 59} for efficient electron regeneration. **Figure 4** shows that the HOMO energies of the studied dyes are -5.31 , -5.13 , -5.23 , and -5.14 eV for **An1–An4**, respectively. Thus, there is a sufficient driving force for fast and efficient regeneration of the oxidized dye. Relatively large energy gaps between the LUMO energies of these dyes and the semiconductor CB together with the low lying HOMO of the I^-/I_3^- redox couple would be beneficial to photovoltaic conversion.

3.4 Absorption spectra and light harvesting properties

To determine the dye optical absorption characteristics and electronic transitions in CH_2Cl_2 solvent, we performed TD-DFT calculations using the CAM-B3LYP function under the C-PCM continuum solvation model. The calculated maximum absorption wavelengths (λ_{abs}), oscillator strengths (f), electronic transitions, and light harvesting efficiencies (*LHE*) are listed in **Table 2**. Simulated absorptionspectra for the **An1–An4** dyes are shown in **Figure 5**.

The dyes exhibit two major absorption regions at roughly 292–374 and 450–562 nm. We ascribe the absorption bands below 400 nm to $\pi-\pi^*$ transitions of the conjugated molecules. Bands in the longer wavelength region greater than 400 nm commonly arise from ICT transitions, which are an important band for DSSC applications. **Figure 5** shows that **An1** exhibits λ_{abs} at 374 nm (**Table S1**), which is below 400 nm, and thus ICT is probably absent due to the large dihedral angles measured at the position 9 and 10 of anthracene for **An1**, as discussed in **Section 3.1**.

It is interesting to compare the optical properties of the **An1** dye without TB, and the **An2–An4** dyes, which incorporate TB as a π linker. The dye λ_{abs} values fall in the order **An4** (562 nm) > **An3** (490 nm) > **An2** (450 nm) > **An1** (374 nm). The inclusion of TB in the

π -conjugation chain causes red shift of the dye λ_{abs} values. Compared to λ_{abs} of **An1** dye at 374 nm, the red shifts of the λ_{abs} are calculated to be 76, 116, and 188 nm for **An2**, **An3**, and **An4**, respectively. These results clearly indicate that TB significantly extends the π -conjugation length, resulting in emergence of strongly favorable ICT. The extension of the linker conjugation length is further confirmed by the L distance, which increases in the order **An2** (8.18 Å) < **An3** (10.72 Å) < **An4** (17.53 Å). **An4** exhibits the broadest and most intense absorption spectrum. Therefore, **An4** is expected to be the most suitable dye for DSSC applications.

We also calculated light harvesting efficiency (LHE) to determine the extent of light absorption and J_{sc} values for the dyes.¹⁹ The LHE can be approximated by **Equation 2**.

$$LHE = 1 - 10^{-A} = 1 - 10^{-f} \quad (2)$$

$$J_{\text{sc}} = \int LHE(\lambda) \Phi_{\text{inject}} \eta_{\text{collect}} d\lambda \quad (3)$$

Where, $A(f)$ is the absorption intensity (oscillator strength) of the dye, associated with λ_{abs} , Φ_{inject} is the quantum yield of electron injection, and η_{collect} represents electron collection efficiency. The LHE against absorption wavelength are plotted in **Figure 6**, while the calculated LHE values at maximum wavelengths are listed in **Table 2**. The **An2–An4** dyes with triple bond-modified linkers show greater LHE values than the **An1** dye without TB. LHE curves show that after TB-modification, light harvesting efficiency remarkably increases. The **An4** is expected to be potential sensitizers for harvesting light along high photo flux spectrum which extend to near infrared region. Because the LHE is proportional to J_{sc} , as shown in **Equation 3**, we expect that the **An4** dye which is superior to other compounds, will also have the greatest J_{sc} value, and thus, use of **An4** would provide the greatest efficiency in DSC applications.

3.5 Driving force (ΔG^{inject}) and the electron injection process

For electron injection processes in DSSCs, the free energy change (ΔG^{inject}) is an important parameter for characterizing the rate and efficiency of the reaction. **Figure 7** shows the free energy change (ΔG^{inject}) that occurs as a result of electron injection in a DSSC. The initial state of the reaction is the excited electron of dye adsorbed on a TiO_2 surface, and the final state corresponds to the injected electron on TiO_2 surface. The ΔG^{inject} can be obtained from **Equation 4**, representing the energy difference between these initial and final states, where E_{ox}^* representing to the photo-induced excited states of the organic dyes and E_{CB} representing to reduction potential of the TiO_2 semiconductor. The E_{ox}^* can be computed from **Equation 5**, where E_{ox} is the redox potential of the dye in the ground state and λ_{abs} is the absorption energy.

$$\Delta G^{\text{inject}} = E_{\text{ox}}^* - E_{\text{CB}} \quad (4)$$

$$E_{\text{ox}}^* = E_{\text{ox}} - \lambda_{\text{abs}} \quad (5)$$

Taking into account the ΔG^{inject} listed in **Table 2**, we found that all ΔG^{inject} values are negative with sufficiently high ΔG^{inject} value (>0.2 eV) to obtain a high efficiency of electron injection in DSSCs,⁶⁰ the electron injection process thermodynamically possible (i.e., $\Delta G^{\text{inject}} < 0$), confirming that the LUMO level of the dye must lie above the TiO_2 CB edge. Therefore, photo-excitation should be capable of producing sufficiently excited electrons for injection into the TiO_2 conduction bands. To enable sufficient driving force for electron injection, a good overlap of the excited states of the dye and the potential of the TiO_2 is crucial.⁶¹

To further study the structure of the dye sensitizer-semiconductor interface and the process of electron transfer from the dye sensitizer to semiconductor surface, we modeled the **An1-**, **An2-**, **An3-**, and **An4-TiO₂** adsorption complexes (**Dyes-TiO₂**) using the Dmol³ computer program. **Figure 8** shows the optimized structures, and **Table 3** lists adsorption

energies (E_{ads}). As shown, the optimized adsorbed-dye structures are positioned almost perpendicular to the TiO_2 surface, linked by two O-Ti bonds in a bidentate-bridging adsorption mode. The calculated E_{ads} values for **Dyes-TiO₂** are in the range 19–21 kcal/mol, indicating strong interactions between the dyes and the TiO_2 surface. In addition, to consider dipole moment of the dyes adsorbed onto $(\text{TiO}_2)_{38}$ cluster, we made the C2 axis of the carboxylate in the dye parallel to the y-axis, and the semiconductor surface is parallel to the xz plane as shown in **Figure 8**. The calculated dipole moments along y-axis (μ_y) of dyes increased in the order of **An1** (21.730) < **An2** (24.52) < **An3** (25.04) < **An4** (26.02), respectively. This calculated result confirms the strong intramolecular charge transfer (ICT) property of TB modified-linker dyes (**An2**, **An3**, **An4**) which expected to perform higher electron injection efficiency than **An1** dye without TB.

Upon excitation, electronic coupling and electron transfer take place between the LUMO on the dye and the CB on TiO_2 . Thus, it is important to analyze the frontier molecular orbitals of the **Dyes-TiO₂** complexes, and for the LUMO in particular. To get more insights into the orbital charge densities for frontier molecular orbitals of the **Dyes-TiO₂** complexes, the optimized geometries of the **Dyes-TiO₂** complexes from DMol³ were further calculated the electronic transition energies with TD-DFT calculations using CAM-B3LYP functional with the 3-21G(d) basis as implemented in the GAUSSIAN 09 program. The results are shown in **Table 3**. **Figure 9** shows selected isosurface frontier molecular orbitals, including HOMO, LUMO, and other interacting orbitals of the **Dyes-TiO₂** complexes. For the **An1-TiO₂** adsorption complex (**Figure 9a**), the electronic transition corresponds to a HOMO→LUMO interaction. The HOMO electron density localizes on the Cbz-Cbz donor group, while electron density in the LUMO is located on the TiO_2 surface. However, this transition does not represent the direction of electron transfer, because there is no electron density located at the cyanoacrylic acid anchoring group for the LUMO of the dye acceptor.

This calculated result probably arises because of the twisted anthracene geometry in **An1**, with dihedral angles at the 9- and 10-positions that are almost perpendicular to the cyanoacrylic acid anchoring plane, and which result in suppression of electron transfer.

For the **An2-TiO₂** adsorption complex (**Figure 9b**), the electronic transition corresponds to the linear combination of HOMO→LUMO+59 and HOMO→LUMO+60. The electron distribution of the HOMO mainly localizes on the anthracene moiety and the adjacent carbazole unit. This calculated result is consistent with the incorporation of TB between 9-anthracene and the carbazole donor, which results in a significantly decreased dihedral angle between anthracene and the adjacent carbazole group, and consequently improved electron transfer from the carbazole donor onto anthracene. However, electron density cannot extend past the 10-position because of the large dihedral angle, and consequently, there is no electron density located on the cyanoacrylic acid anchoring group for LUMO+59 or LUMO+60. Thus, this transition also could not represent a route for electron transfer from the dye to the TiO₂ surface.

In contrast, **An3-TiO₂** and **An4-TiO₂** adsorption complexes (**Figure 9c** and **9d**) with TB at positions 10 and 9,10 on anthracene, respectively, have much smaller dihedral angles at the 10-position and are essentially planar. Consequently, electron transfer to the TiO₂ surface via the cyanoacrylic-anchoring group can occur. On the other hand, in order to have back electron transfer, the electron from the TiO₂ needs to enter the dye via the anchor. Therefore, if the LUMO of the dye is considerably more localized on the anchors and has a small contribution from the chromophoric unit, back electron transfer will be hampered.⁶² The charge recombination is found to be less probable in **An-3** and **An-4** due to large contributions of the anchoring atoms to the LUMO orbital density compared to **An-1** and **An-2**, see Figure 9.

In order to understand electron injection mechanism we analyzed the energy level of the **An-3** and **An-4** dyes before and after interacting with the $(\text{TiO}_2)_{38}$ cluster (**Figure S1**), representing a schematic description of the electronic structure for the free dyes, bare TiO_2 and dye@ TiO_2 system. We found that the LUMO level of the dye@ TiO_2 complex is lower than that for the free dye, which is above the CB level of the TiO_2 indicating the efficient electron transfer from the dye to the semiconductor surface in DSCs. As shown, the HOMO-1 electron distribution for **An3-TiO₂** and HOMO for **An4-TiO₂** are mainly localized on the anthracene moiety, with slight delocalization to the anchoring group, while the patterns of LUMO+21 for **An3-TiO₂** and LUMO+20 for **An4-TiO₂**, show that the electron distribution is delocalized across both the TiO_2 surface and the cyanoacrylic-anchoring group. These distributions represent electron transfer from the dye via the anchoring group to the TiO_2 surface as a consequence of direct electron injection. The effects of connecting the anchoring group to anthracene at different positions for **An3-TiO₂** (9-position) and **An4-TiO₂** (9,10-positions) adsorption complexes are similar. The reason is that electron density can transfer from anthracene to the TiO_2 surface through the small dihedral angle between anthracene and thiophene at the 10-position. Thus, the presence of **TB** plays a key role in electron transfer and in the injection mechanism at the $(\text{TiO}_2)_{38}$ surface.

4 Conclusions

In summary, we used computational methods to design and investigate a series of three anthracene-based dyes, **An2–An4**, with a TB-modified π -conjugated linker and compared these to the **An1** dye without TB substitution. Interestingly, all three anthracene-based sensitizers **An2–An4** showed significant decreases in the dihedral angle between the anthracene unit and its substituents at the 9,10-positions, resulting in a nearly planar molecular geometry for each dye. The presence of a planar structure greatly affects the absorption spectra, which broadens with increasing coplanarity distance (L). Furthermore,

molecular coplanarity of with the π -conjugated linker has a significant effect on electron distribution overlap on anthracene, which facilitates ICT. According to calculated absorption spectra, the **An4** dye exhibits a prominent red-shift in its absorption peak, which is beneficial to its light-harvesting efficiency. The calculated electronic transitions for the dye-(TiO₂)₃₈ clusters revealed that dyes bearing a TB moiety directly linked between anthracene and the anchoring group, exhibit electron injection from the dye to the TiO₂ surface. These results indicate that inclusion of a triple bond-modified π -conjugated linker in these dyes during synthesis is necessary for the construction of high-efficiency organic sensitizers.

Acknowledgements

The authors acknowledge and thank the Department of Chemistry at Ubon Ratchathani and Chiang Mai Universities for providing access to their computing resources. Financial support from the Human Resource Development in Science Project (Science Achievement Scholarship of Thailand, SAST), Thailand Research Fund (grant number RSA5780048) and the Center of Excellence for Innovation in Chemistry (PERCH-CIC), the office of the Higher Education Commission, and the Ministry of Education are gratefully acknowledged.

References

1. B. O'Regan and M. Gratzel, *Nature*, 1991, **353**, 737-740.
2. M. Grätzel, *Journal of Photochemistry and Photobiology C: Photochemistry Reviews*, 2003, **4**, 145-153.
3. L. M. Peter, *The Journal of Physical Chemistry Letters*, 2011, **2**, 1861-1867.
4. K. Srinivas, K. Yesudas, K. Bhanuprakash, V. J. Rao and L. Giribabu, *The Journal of Physical Chemistry C*, 2009, **113**, 20117-20126.
5. C. Teng, X. Yang, C. Yang, S. Li, M. Cheng, A. Hagfeldt and L. Sun, *The Journal of Physical Chemistry C*, 2010, **114**, 9101-9110.
6. J. Xu, L. Wang, G. Liang, Z. Bai, L. Wang, W. Xu and X. Shen, *Spectrochimica Acta Part A: Molecular and Biomolecular Spectroscopy*, 2011, **78**, 287-293.
7. Z. Chen, F. Li and C. Huang, *Current Organic Chemistry*, 2007, **11**, 1241-1258.
8. M. Gratzel, *Inorg. Chem.*, 2005, **44**, 6841-6851.
9. H. Zhang, J. Fan, Z. Iqbal, D.-B. Kuang, L. Wang, D. Cao and H. Meier, *Dyes and Pigments*, 2013, **99**, 74-81.

10. J. Zhang, H.-B. Li, Y. Geng, S.-Z. Wen, R.-L. Zhong, Y. Wu, Q. Fu and Z.-M. Su, *Dyes and Pigments*, 2013, **99**, 127-135.
11. L.-L. Tan, L.-J. Xie, Y. Shen, J.-M. Liu, L.-M. Xiao, D.-B. Kuang and C.-Y. Su, *Dyes and Pigments*, 2014, **100**, 269-277.
12. A. Yella, R. Humphry-Baker, B. F. E. Curchod, N. Ashari Astani, J. Teuscher, L. E. Polander, S. Mathew, J.-E. Moser, I. Tavernelli, U. Rothlisberger, M. Grätzel, M. K. Nazeeruddin and J. Frey, *Chemistry of Materials*, 2013, **25**, 2733-2739.
13. H. Tian, X. Yang, R. Chen, Y. Pan, L. Li, A. Hagfeldt and L. Sun, *Chemical Communications*, 2007, 3741-3743.
14. C.-J. Yang, Y. J. Chang, M. Watanabe, Y.-S. Hon and T. J. Chow, *Journal of Materials Chemistry*, 2012, **22**, 4040-4049.
15. L. Ducasse, F. Castet, R. Méreau, S. Nénon, J. Idé, T. Toupance and C. Olivier, *Chemical Physics Letters*, 2013, **556**, 151-157.
16. A. S. Hart, C. B. Kc, H. B. Gobeze, L. R. Sequeira and F. D'Souza, *ACS Applied Materials & Interfaces*, 2013, **5**, 5314-5323.
17. H. W. Ham and Y. S. Kim, *Thin Solid Films*, 2010, **518**, 6558-6563.
18. J. Zhang, Y.-H. Kan, H.-B. Li, Y. Geng, Y. Wu and Z.-M. Su, *Dyes and Pigments*, 2012, **95**, 313-321.
19. W. Fan, D. Tan and W.-Q. Deng, *ChemPhysChem*, 2012, **13**, 2051-2060.
20. C.-Y. Lin, Y.-C. Wang, S.-J. Hsu, C.-F. Lo and E. W.-G. Diau, *The Journal of Physical Chemistry C*, 2009, **114**, 687-693.
21. Y.-S. Yen, Y.-C. Chen, H.-H. Chou, S.-T. Huang and J. T. Lin, *Polymers*, 2012, **4**, 1443-1461.
22. R. Yeh-Yung Lin, H.-W. Lin, Y.-S. Yen, C.-H. Chang, H.-H. Chou, P.-W. Chen, C.-Y. Hsu, Y.-C. Chen, J. T. Lin and K.-C. Ho, *Energy & Environmental Science*, 2013, **6**, 2477-2486.
23. Y.-Z. Lin, C. H. Huang, Y. J. Chang, C.-W. Yeh, T.-M. Chin, K.-M. Chi, P.-T. Chou, M. Watanabe and T. J. Chow, *Tetrahedron*, 2014, **70**, 262-269.
24. J. Yang, F. Guo, J. Hua, X. Li, W. Wu, Y. Qu and H. Tian, *Journal of Materials Chemistry*, 2012, **22**, 24356-24365.
25. S. J. K. Dong Uk Heo, Beom Jin Yoo, Boeun Kim, Min Jae Ko, Min Ju Cho, Dong Hoon Choi, *Bulletin of the Korean Chemical Society* 2013, **34**, 1081 - 1088.
26. A. Hagfeldt, G. Boschloo, L. Sun, L. Kloo and H. Pettersson, *Chemical Reviews*, 2010, **110**, 6595-6663.
27. K. R. Justin Thomas, P. Singh, A. Baheti, Y.-C. Hsu, K.-C. Ho and J. T. s. Lin, *Dyes and Pigments*, 2011, **91**, 33-43.
28. H. Li, Y. Yang, Y. Hou, R. Tang, T. Duan, J. Chen, H. Wang, H. Han, T. Peng, X. Chen, Q. Li and Z. Li, *ACS Sustainable Chemistry & Engineering*, 2014, **2**, 1776-1784.
29. C. Yan, W. Ma, Y. Ren, M. Zhang and P. Wang, *ACS Applied Materials & Interfaces*, 2015, **7**, 801-809.
30. L. Yang, Y. Ren, Z. Yao, C. Yan, W. Ma and P. Wang, *The Journal of Physical Chemistry C*, 2015, **119**, 980-988.
31. C.-K. Tai, Y.-J. Chen, H.-W. Chang, P.-L. Yeh and B.-C. Wang, *Computational and Theoretical Chemistry*, 2011, **971**, 42-50.
32. Z. Cai-Rong, L. Zi-Jiang, C. Yu-Hong, C. Hong-Shan, W. You-Zhi and Y. Li-Hua, *Journal of Molecular Structure: THEOCHEM*, 2009, **899**, 86-93.
33. C.-R. Zhang, L. Liu, Z.-J. Liu, Y.-L. Shen, Y.-T. Sun, Y.-Z. Wu, Y.-H. Chen, L.-H. Yuan, W. Wang and H.-S. Chen, *Journal of Molecular Graphics and Modelling*, 2012, **38**, 419-429.
34. S.-L. Chen, L.-N. Yang and Z.-S. Li, *Journal of Power Sources*, 2013, **223**, 86-93.
35. A. Irfan, *Materials Chemistry and Physics*, 2013, **142**, 238-247.
36. F. Labat, T. Le Bahers, I. Ciofini and C. Adamo, *Accounts of Chemical Research*, 2012, **45**, 1268-1277.
37. S. Jungsttiwong, T. Yakhantip, Y. Surakhot, J. Khunchalee, T. Sudyoosuk, V. Promarak, N. Kungwan and S. Namuangruk, *Journal of Computational Chemistry*, 2012, **33**, 1517-1523.
38. T. Yakhantip, S. Jungsttiwong, S. Namuangruk, N. Kungwan, V. Promarak, T. Sudyoosuk and P. Kochpradist, *Journal of Computational Chemistry*, 2011, **32**, 1568-1576.

39. S. Namuangruk, R. Fukuda, M. Ehara, J. Meeprasert, T. Khanasa, S. Morada, T. Kaewin, S. Jungstittiwong, T. Sudyoadsuk and V. Promarak, *The Journal of Physical Chemistry C*, 2012, **116**, 25653-25663.
40. R. Tarsang, V. Promarak, T. Sudyoadsuk, S. Namuangruk and S. Jungstittiwong, *Journal of Photochemistry and Photobiology A: Chemistry*, 2014, **273**, 8-16.
41. N. Kungwan, P. Khongpracha, S. Namuangruk, J. Meeprasert, C. Chitpakdee, S. Jungstittiwong and V. Promarak, *Theoretical Chemistry Accounts*, 2014, **133**, 1-14.
42. M. Frisch, G. Trucks, H. Schlegel, G. Scuseria, M. Robb, J. Cheeseman, G. Scalmani, V. Barone, B. Mennucci, G. Petersson, H. Nakatsuji, M. Caricato, X. Li, H. Hratchian, A. Izmaylov, J. Bloino, G. Zheng, J. Sonnenberg, M. Hada, M. Ehara, K. Toyota, R. Fukuda, J. Hasegawa, M. Ishida, T. Nakajima, Y. Honda, O. Kitao, H. Nakai, T. Vreven, J. Montgomery, J. Peralta, F. Ogliaro, M. Bearpark, J. Heyd, E. Brothers, K. Kudin, V. Staroverov, R. Kobayashi, J. Normand, K. Raghavachari, A. Rendell, J. Burant, S. Iyengar, J. Tomasi, M. Cossi, N. Rega, J. Millam, M. Klene, J. Knox, J. Cross, V. Bakken, C. Adamo, J. Jaramillo, R. Gomperts, R. Stratmann, O. Yazyev, A. Austin, R. Cammi, C. Pomelli, J. Ochterski, R. Martin, K. Morokuma, V. Zakrzewski, G. Voth, P. Salvador, J. Dannenberg, S. Dapprich, A. Daniels, Farkas, J. Foresman, J. Ortiz, J. Cioslowski and D. Fox, *Gaussian 09, Revision C.01*, Gaussian, Inc., Wallingford CT, 2009.
43. A. D. Becke, *The Journal of Chemical Physics*, 1993, **98**, 1372-1377.
44. G. A. Petersson, A. Bennett, T. G. Tensfeldt, M. A. Al-Laham, W. A. Shirley and J. Mantzaris, *The Journal of Chemical Physics*, 1988, **89**, 2193-2218.
45. M. Pastore, E. Mosconi, F. De Angelis and M. Grätzel, *The Journal of Physical Chemistry C*, 2010, **114**, 7205-7212.
46. S. I. Gorelsky and A. B. P. Lever, *Journal of Organometallic Chemistry*, 2001, **635**, 187-196.
47. M. K. Nazeeruddin, F. De Angelis, S. Fantacci, A. Selloni, G. Viscardi, P. Liska, S. Ito, B. Takeru and M. Grätzel, *Journal of the American Chemical Society*, 2005, **127**, 16835-16847.
48. B. Delley and D. E. Ellis, *The Journal of Chemical Physics*, 1982, **76**, 1949-1960.
49. S. Namuangruk, K. Sirithip, R. Rattanawan, T. Keawin, N. Kungwan, T. Sudyoadsuk, V. Promarak, Y. Surakhot and S. Jungstittiwong, *Dalton Transactions*, 2014, **43**, 9166-9176.
50. S. Namuangruk, J. Meeprasert, S. Jungstittiwong, V. Promarak and N. Kungwan, *Theoretical Chemistry Accounts*, 2014, **133**, 1-15.
51. R. Tarsang, V. Promarak, T. Sudyoadsuk, S. Namuangruk, N. Kungwan and S. Jungstittiwong, *ChemPhysChem*, 2014, **15**, 3809-3818.
52. S. Jungstittiwong, R. Tarsang, T. Sudyoadsuk, V. Promarak, P. Khongpracha and S. Namuangruk, *Organic Electronics*, 2013, **14**, 711-722.
53. E. Ronca, M. Pastore, L. Belpassi, F. Tarantelli and F. De Angelis, *Energy & Environmental Science*, 2013, **6**, 183-193.
54. M. Khoudiakov, A. R. Parise and B. S. Brunshwig, *Journal of the American Chemical Society*, 2003, **125**, 4637-4642.
55. Y.-X. Weng, Y.-Q. Wang, J. B. Asbury, H. N. Ghosh and T. Lian, *The Journal of Physical Chemistry B*, 2000, **104**, 93-104.
56. F. D. Angelis, S. Fantacci and A. Selloni, *Nanotechnology*, 2008, **19**, 424002.
57. F. De Angelis, S. Fantacci, E. Mosconi, M. K. Nazeeruddin and M. Grätzel, *The Journal of Physical Chemistry C*, 2011, **115**, 8825-8831.
58. D. Cahen, G. Hodes, M. Grätzel, J. F. Guillemoles and I. Riess, *The Journal of Physical Chemistry B*, 2000, **104**, 2053-2059.
59. W. Sang-aroon, S. Saekow and V. Amornkitbamrung, *Journal of Photochemistry and Photobiology A: Chemistry*, 2012, **236**, 35-40.
60. R. Katoh and A. Furube, *Journal of Photochemistry and Photobiology C: Photochemistry Reviews*, 2014, **20**, 1-16.
61. J. Wiberg, T. Marinado, D. P. Hagberg, L. Sun, A. Hagfeldt and B. Albinsson, *The Journal of Physical Chemistry B*, 2010, **114**, 14358-14363.
62. S. M. Pratik and A. Datta, *Phys. Chem. Chem. Phys.*, 2013, **15**, 18471-18481.

Figure Captions

- Figure 1** Sketch map of the studied dyes **An1** – **An4**.
- Figure 2** (a) The molecular structures were categorized into three parts of donor, linker, and acceptor, (b) Optimized structures of the studied dyes **An1** – **An4** calculated by B3LYP/6-31G(d,p) level of theory.
- Figure 3** The frontier molecular orbitals of HOMO (left) and LUMO (middle), and the charge density difference between the ground- and excited-state (right) of the studied dyes calculated under TD-CAM-B3LYP/6-31G(d,p). The purple represent where the electrons are decreased and the yellow represents where the electrons are increased.
- Figure 4** Computed HOMO-LUMO energy levels for the studied dyes **An1** – **An4** at the TD-CAM-B3LYP/6-31G(d,p), together with the TiO₂ conduction band edge and the I/I₃⁻ redox potential.
- Figure 5** The calculated UV-Vis spectra of **An1** –**An4** dyes using TD-CAM-B3LYP/6-31G(d,p) model in CH₂Cl₂ solution.
- Figure 6** LHE curves of **An1** –**An4** dyes along with photon flux spectrum at ASTM-G173 AM1.5G.
- Figure 7** Schematic of free energy change (ΔG^{inject}) producing from the energy difference between E_{LUMO} and E_{CB} .
- Figure 8** Optimized structures of **An1**-, **An2**-, **An3**- and **An4-TiO₂** adsorption complexes calculated by PBE/DNP in the Dmol³.
- Figure 9** Electronic transitions of a) **An1-TiO₂**, b) **An2-TiO₂**, c) **An3-TiO₂** and d) **An4-TiO₂** adsorption complexes calculated by TD-CAM-B3LYP/3-21G(d).
- Figure S1** Schematic energy diagram of the free dyes, bare TiO₂ and dye@TiO₂ system at the optimized structures by Dmol³.

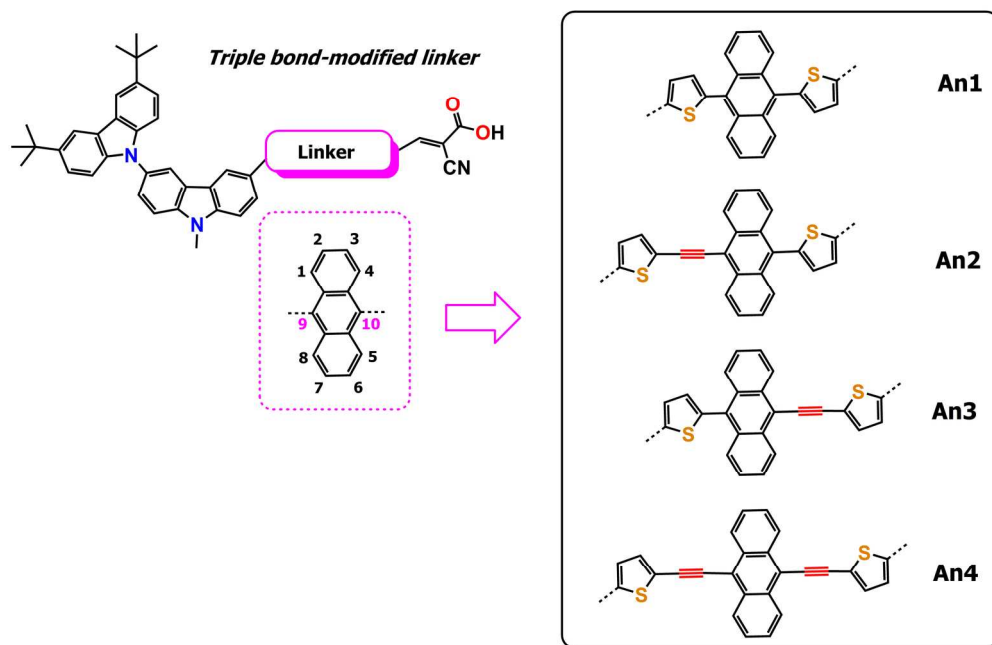


Figure 1 Sketch map of the studied dyes An1 – An4.
89x58mm (600 x 600 DPI)

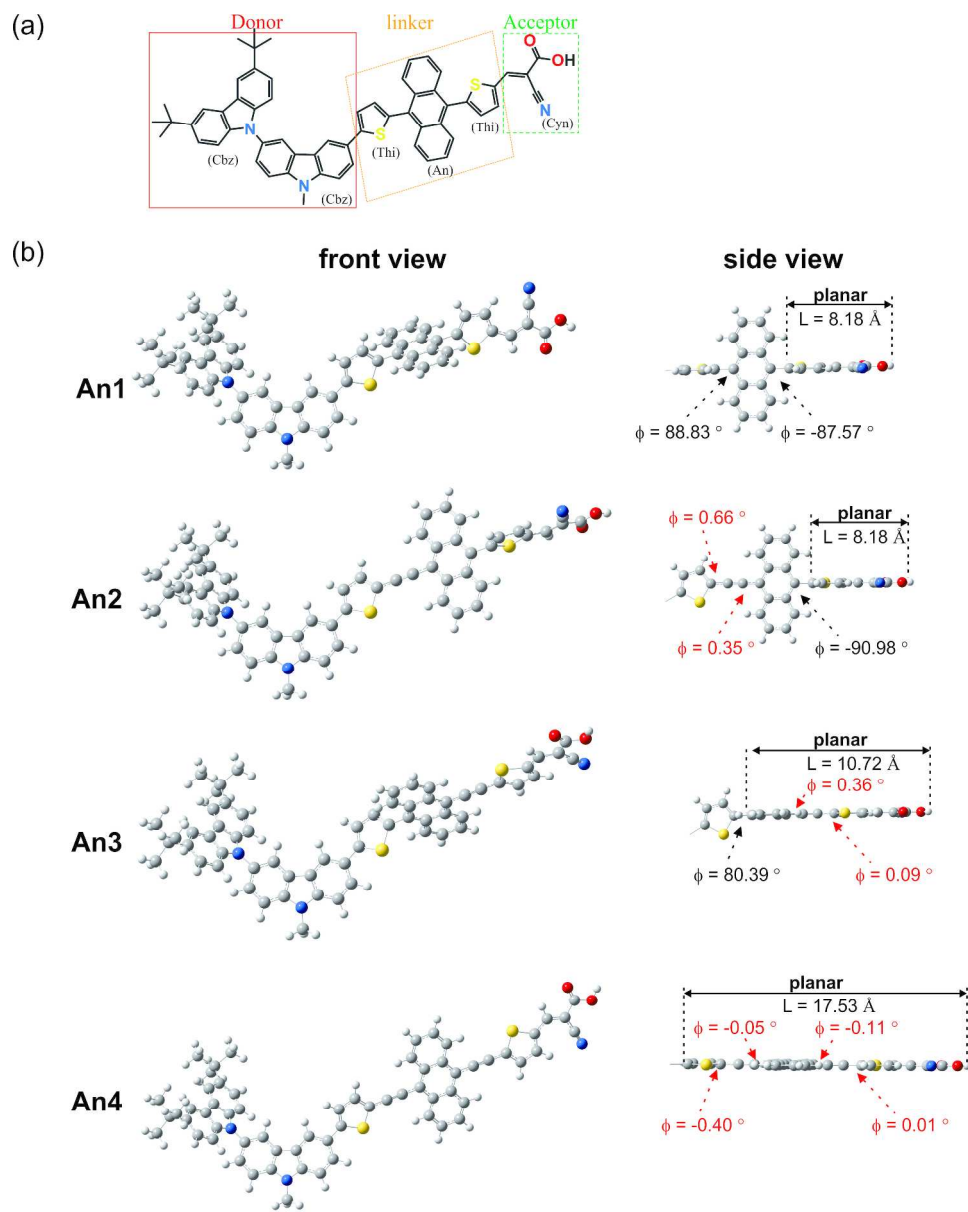


Figure 2 (a) The molecular structures were categorized into three parts of donor, linker, and acceptor, (b) Optimized structures of the studied dyes An1 – An4 calculated by B3LYP/6-31G(d,p) level of theory. 302x376mm (300 x 300 DPI)

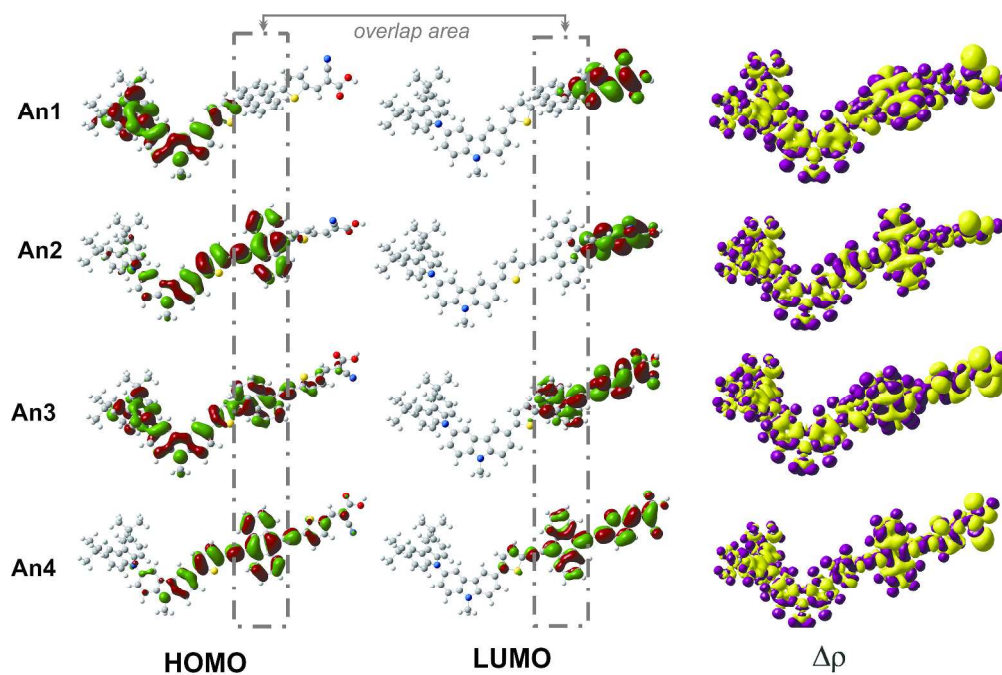


Figure 3 The frontier molecular orbitals of HOMO (left) and LUMO (middle), and the charge density difference between the ground- and excited-state (right) of the studied dyes calculated under TD-CAM-B3LYP/6-31G(d,p). The purple represent where the electrons are decreased and the yellow represents where the electrons are increased.
474x317mm (300 x 300 DPI)

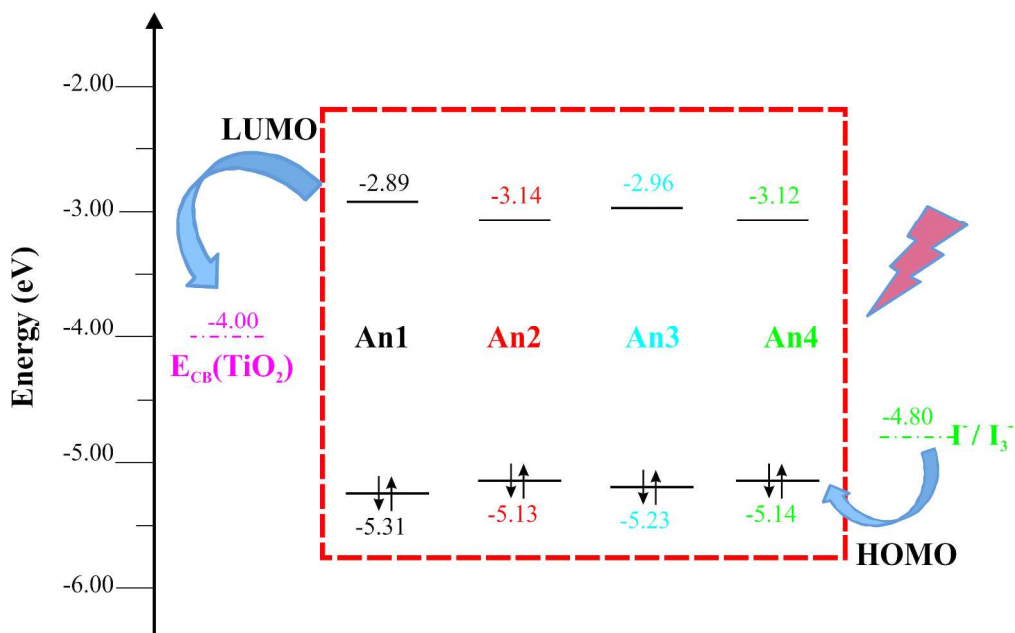


Figure 4. Computed HOMO-LUMO energy levels for the studied dyes An1 – An4 at the TD-CAM-B3LYP/6-31G(d,p), together with the TiO₂ conduction band edge and the I⁻/I₃⁻ redox potential.
404x253mm (300 x 300 DPI)

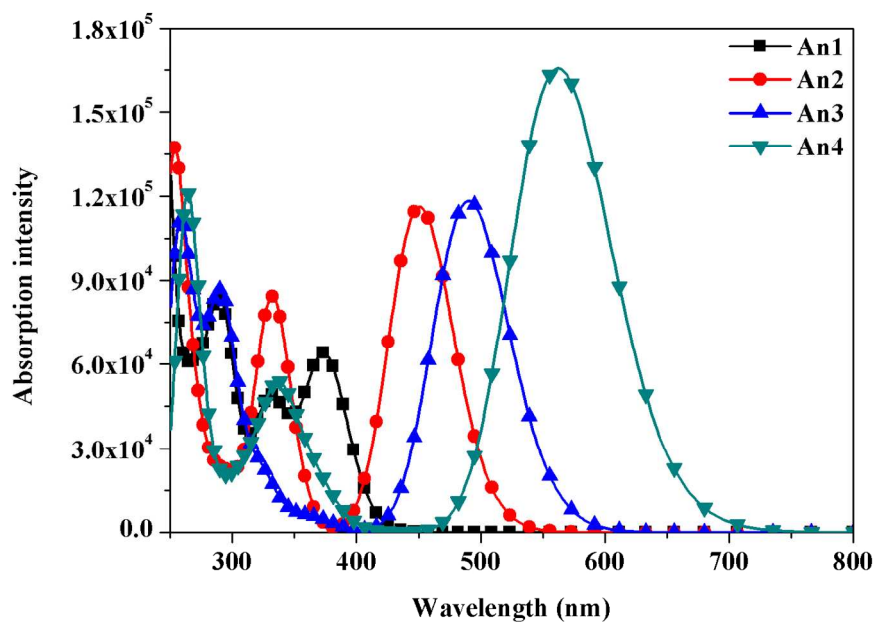


Figure 5 The calculated UV-Vis spectra of An1 –An4 dyes using TD-CAM-B3LYP/6-31G(d,p) model in CH₂Cl₂ solution.

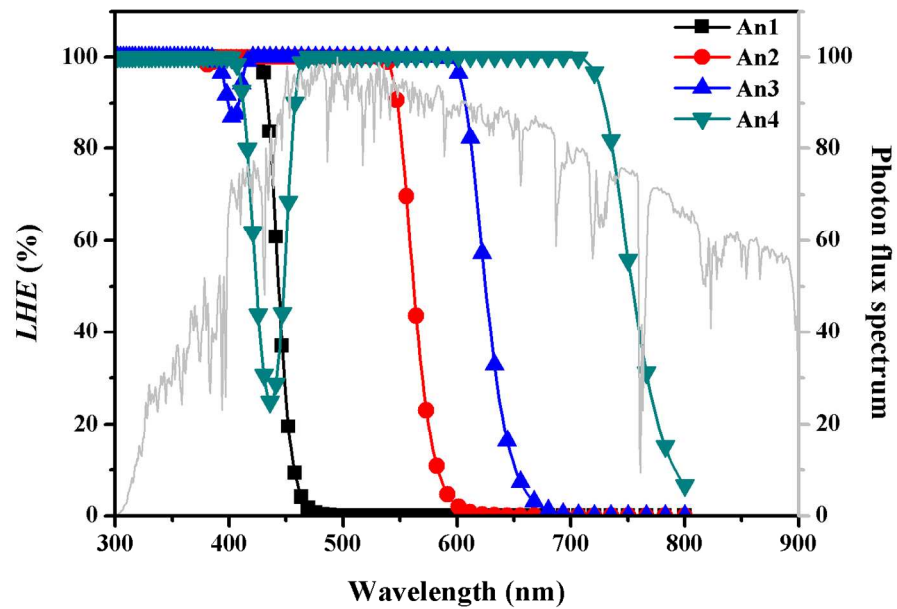


Figure 6 LHE curves of An1 –An4 dyes along with photon flux spectrum at ASTM-G173 AM1.5G.

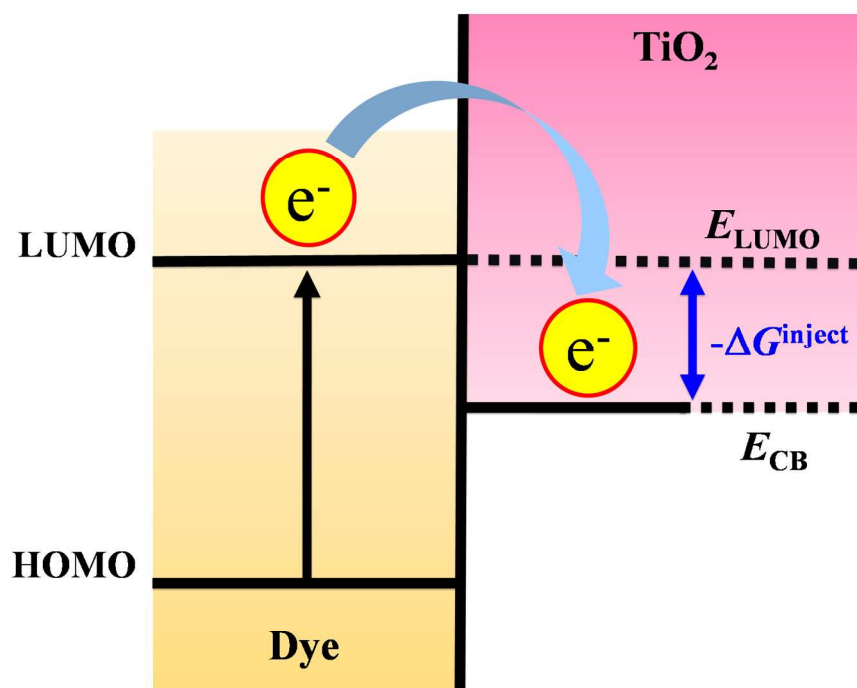


Figure 7 Schematic of free energy change (ΔG^{inject}) producing from the energy difference between ELUMO and ECB.

500x378mm (96 x 96 DPI)

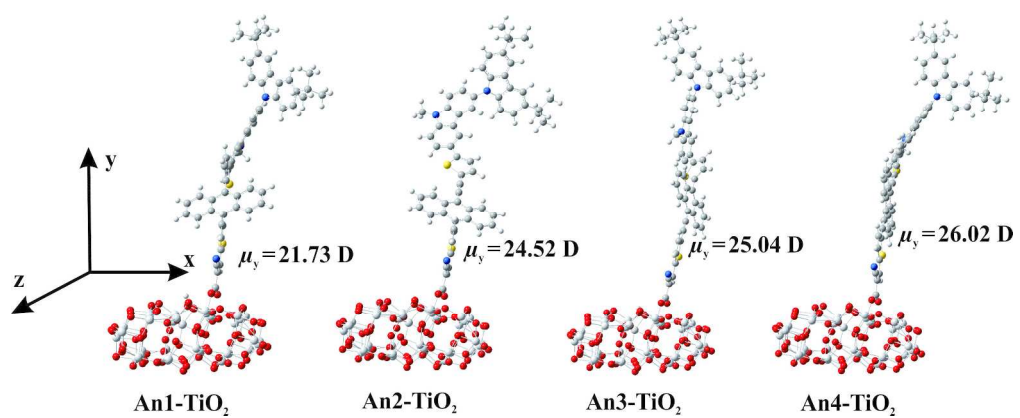


Figure 8 Optimized structures of An1-, An2-, An3- and An4-TiO₂ adsorption complexes calculated by PBE/DNP in the Dmol3.
241x97mm (300 x 300 DPI)

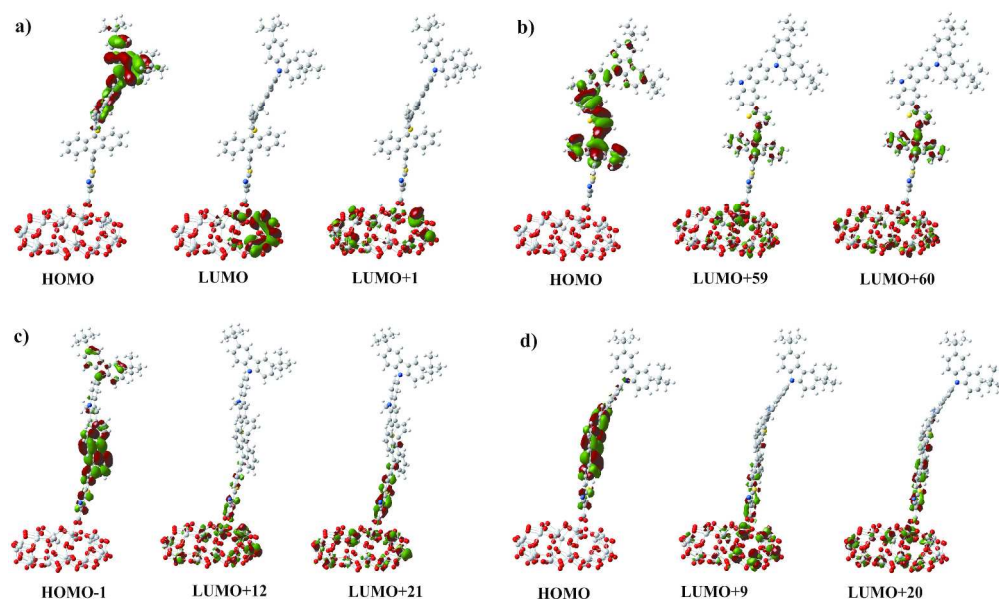


Figure 9 Electronic transitions of a) An1-TiO₂, b) An2-TiO₂, c) An3-TiO₂ and d) An4-TiO₂ adsorption complexes calculated by TD-CAM-B3LYP/3-21G(d).
352x208mm (300 x 300 DPI)

Table 1 Selected bond lengths (r , Å) and dihedral angles (ϕ , degree) for optimized structures of dyes **An1–An4** calculated at the B3LYP/6-31G(d,p) level of theory.

Dyes	Donor	Donor- Linker			Linker			Linker-Acceptor	
	Cbz-Cbz	Cbz-Thi	Thi-An	Thi-TB	TB-An	An-TB	TB-Thi	An-Thi	Thi-Cyn
Bond length (r)									
An1	1.42	1.46	1.48					1.48	1.43
An2	1.42	1.46		1.40	1.42			1.48	1.43
An3	1.42	1.46	1.48			1.41	1.40		1.43
An4	1.42	1.46		1.40	1.41	1.41	1.40		1.43
Dihedral angle (ϕ)									
An1	59.21	29.20	88.83					-87.57	0.19
An2	59.98	-27.92		0.66	0.35			-90.98	-0.13
An3	58.72	-29.68	80.39			0.36	0.09		-0.15
An4	58.26	-37.36		0.40	0.05	0.11	-0.01		-0.08

Cbz = Carbazole, Thi = Thiophene, An = Anthracene, TB = Triple bond, Cyn = Cyanoacrylic acid

Table 2 The maximum absorption wavelength (λ_{abs}), oscillator strength (f), light harvesting efficiency (LHE), electron injection driving force (ΔG^{inject}) and transition compositions of **An1- An4** dyes, calculated by TD-CAM-B3LYP/6-31G(d,p) in CH_2Cl_2 solution (C-PCM model).

Dyes	μ_y^a (Debye)	λ_{abs} , nm(eV)	f	LHE^b	E_{ox}^c	$\Delta G^{\text{inject}d}$	Transition compositions
An1	6.30	374 (3.31)	0.8596	0.86	2.01	-1.99	(+0.62) H-1→L+1 (-0.21) H-2→L+1
An2	7.25	450 (2.75)	1.6038	0.97	2.39	-1.61	(+0.63) H→L+1 (+0.22) H-1→L+1
An3	7.47	490 (2.53)	1.6325	0.98	2.71	-1.29	(+0.51) H-1→L+1 (-0.40) H→L
An4	9.52	562 (2.21)	2.2861	0.99	2.92	-1.08	(+0.63) H→L (-0.17) H→L+1

^a μ_y is dipole moment in the direction perpendicular to the TiO_2 surface

^b $LHE = 1 - 10^{-A} = 1 - 10^{-f}$

^c $E_{\text{ox}}^* = E_{\text{ox}} - \lambda_{\text{abs}}$

^d $\Delta G^{\text{inject}} = E_{\text{ox}}^* - E_{\text{CB}}$

Table 3 The calculated adsorption energy (E_{ads}) obtained using the Dmol³ computer program. Excitation energies (E_{ex}), oscillator strengths (f), and the transition compositions for **An1-**, **An2-**, **An3-**, and **An4-TiO₂** adsorption complexes, calculated by the TD-CAM-B3LYP/3-21G(d,p) level of theory

Complexes	E_{ads} (kcal/mol)	E_{ex} , eV(nm)	f	Transition compositions
An1-TiO₂	20.72	3.07 (404)	0.5570	(+0.90) H→L
An2-TiO₂	19.58	3.76 (449)	1.6644	(+0.24) H→L+60 (+0.24) H→L+59
An3-TiO₂	19.88	2.50 (495)	2.0339	(+0.26) H-1→L+21 (+0.21) H-1→L+12
An4-TiO₂	20.80	2.19 (566)	2.6740	(+0.26) H→L+9 (+0.26) H→L+20

NOTE: H = HOMMO, H-1 = HOMO-1, H-2 = HOMO-2, ...
L = LUMO, L+1 = LUMO+1, L+2 = LUMO+2, ...